

NOVEMBER 08 2012

## Clutter reduction using Doppler sonar in a harbor environment

T. C. Yang; J. Schindall; Chen-Fen Huang; Jin-Yuan Liu



*J. Acoust. Soc. Am.* 132, 3053–3067 (2012)

<https://doi.org/10.1121/1.4756921>



View  
Online



Export  
Citation

CrossMark



ASA

LEARN MORE

Advance your science and career as a member of the  
**Acoustical Society of America**

# Clutter reduction using Doppler sonar in a harbor environment

T. C. Yang<sup>a)</sup> and J. Schindall

Acoustic Division, Naval Research Laboratory, 4555 Overlook Avenue, Washington DC 20375

Chen-Fen Huang

Institute of Oceanography, National Taiwan University, Taipei 10617, Taiwan

Jin-Yuan Liu<sup>b)</sup>

Institute of Applied Marine Physics and Undersea Technology, National Sun Yat-sen University, Kaohsiung 80424, Taiwan

(Received 18 October 2011; revised 5 September 2012; accepted 11 September 2012)

A high frequency experiment was conducted in the Woods Hole Harbor in Massachusetts to evaluate the effectiveness of Doppler sonar for discriminating targets from reverberation. Using a pulsed linear frequency modulated signal, one finds that the matched filtered outputs are filled with high-level discrete backscattered returns, referred to as clutter, which are often confused with the target echo. The high level non-target returns have an amplitude distribution that is heavy-tailed. Using a Doppler-sensitive binary-phase-shift-keying signal coded with an  $m$ -sequence, the target echo and clutter can be separated by Doppler and delay, and tracked using the Doppler spectrogram (Dopplergram). The Doppler filtered time series show a background reverberation with a Rayleigh-like amplitude distribution, with an improved signal-to-(peak) reverberation ratio compared with that without Doppler filtering. The reduced reverberation level with Doppler processing decreases the probability of false alarm (Pfa) for a given threshold level. Conversely, for a given Pfa, the higher signal-to-(peak) reverberation ratio implies a higher probability of detection. Transmission loss measurement was conducted to estimate some of the system parameters, e.g., the source level and target strength relative to the noise level. [<http://dx.doi.org/10.1121/1.4756921>]

PACS number(s): 43.30.Zk, 43.30.Vh, 43.30.Gv [MS]

Pages: 3053–3067

## I. INTRODUCTION

Many commercial sonar systems have been designed to detect and track divers/swimmers in harbors and coastal areas to prevent terrorist attacks.<sup>1</sup> Underwater vehicles loaded with explosives pose even greater threats. Since underwater intruders are acoustically quiet, detection often relies on target echoes from active sonar operated at high frequencies (tens of kilohertz). The sonar returns are normally displayed in range and bearing referred to as an echograph. It is found that the echograph (using Doppler insensitive waveforms) is full of high level scattered returns, some of them form “tracks” and can be confused with targets.<sup>2</sup> Discrete high level returns that are not target-related are referred to as clutter. Clutter reduction requires novel system solutions, signal-processing techniques,<sup>1,2</sup> and better understanding of the clutter statistics. For example, advanced tracking techniques based on track kinematics have been widely used to analyze the clutter data to detect moving targets. See, for example, Refs. 3 and 4, and references therein. On the other hand, we find, to our knowledge, little analyses on the acoustic properties of the signal and reverberation in harbor environments, nor any capability to model/predict their levels and statistical properties. In general, active sonar can encounter high level reverberation

returns from man-made structures, debris, uneven bottom depth, fish school, etc., in harbor environments. As the sonar resolution improves, scattered returns from discrete objects are more pronounced and can be confused with the targets. In this paper, we investigate the use of a Doppler sonar to discriminate the target from the reverberation.

Most sonar systems use linear frequency modulated (LFM) or hyperbolic frequency modulated (HFM) pulses for range estimation. The HFM pulse is used for its Doppler insensitivity, allowing all Doppler targets to be processed with only one replica. Doppler-sensitive waveforms, such as pulsed sinusoidal waves, have also been used in low frequency active sonar, often in combination with other waveforms, such as HFM. Other Doppler-sensitive waveforms include binary phase-shift keying (BPSK) and Costas signals. For a moving source, the Doppler of the reverberation are bearing (beam angle) dependent. Doisy *et al.* explored the bearing-dependent Doppler to discriminate/suppress reverberation from different look directions using pulsed sinusoidal waves and pulsed trains of frequency-modulated signals.<sup>5,6</sup> Jourdain and Henrioux used BPSK signals to study echo returns from target highlights moving along a rectilinear trajectory.<sup>7,8</sup> The knowledge of the delay-Doppler values for different points allows estimation of target dimensions and longitudinal speed.<sup>7</sup> The phase differences of the peaks of the cross-ambiguity surfaces between two sensors can be used to estimate the target bearing and improve target classification.<sup>8</sup>

An experiment was conducted in the Woods Hole Harbor in Massachusetts to study the acoustic properties of the

<sup>a)</sup>Author to whom correspondence should be addressed. Also at: Institute of Applied Marine Physics and Undersea Technology, National Sun Yat-sen University, Kaohsiung 80424, Taiwan. Electronic mail: tsihyang@gmail.com

<sup>b)</sup>Also at: National Taitung University, Taitung 95092, Taiwan.

reverberation and target echo at high frequencies (50 to 60 kHz) using both Doppler insensitive and sensitive waveforms. One-way transmission loss (TL) was measured as a function of range to aid modeling of the target echo level versus range. One finds that the TL is highly sensitive to the bottom bathymetry. For the active experiment, directional sonar with low sidelobe levels (<-30 dB) was used to minimize reverberation from non-target look directions. In the target look direction, one finds that the reverberation is filled with many high level returns not associated with the target. In this (reverberation-limited) environment, extracting the target echo is often difficult due to interference from reverberation. This motivates us to use Doppler to discriminate (and separate) the target from non-target returns (in the look direction). To improve the range and Doppler resolution, and the processing gain, wideband signals are used during the experiment. The active returns are processed using the wideband ambiguity function (WAF) (described below in Sec. II) referred to as the Doppler analysis/processing. One finds that:

- (1) The high level non-target returns have low Doppler frequencies. They are hypothesized as (back)scattered returns from volume inhomogeneities drifting slowly with the tide. These low-Doppler reverberation returns have a heavy-tailed probability distribution in amplitude.
- (2) The signals from a moving target can be sorted on the basis of their Doppler content, allowing rejection of unwanted signals. Using Doppler processing, the target signal-to-peak-reverberation ratio (SPRR) is significantly improved (>10 dB at times compared with the unfiltered data). The Doppler processed time series contains some residue reverberation whose amplitude envelopes show a Rayleigh-like distribution.
- (3) Doppler processing has a resolution of ~3 Hz at a carrier frequency of 50 kHz using a BPSK signal of 0.26 s duration. This implies that target speed can be measured with an accuracy of 0.1 m/s in the look direction. A swimmer in motion (with speed >0.1 m/s in the look direction) is expected to be identifiable in the Doppler space. An underwater vehicle moving with a speed of a few knots (in the look direction) should be detectable by its Doppler shift with a low probability of false alarm (Pfa), since reverberation is concentrated in the low Doppler space. For example, a “strong” peak in the high Doppler space in individual wideband ambiguity surfaces is a clear indication of a speedy target, even with a few snapshots of data.
- (4) Target tracking in the Doppler space (equivalently target-speed) produces a Dopplergram.<sup>9</sup> The concept is patterned after the Lofargram (or spectrogram) used in passive sonar, where detection is improved by (eyeball) integration along the target spectral peaks. In a Dopplergram, the presence of a “line” in the high Doppler space (say, with >0.5 knot radial speed) is an “unambiguous” indication of a speedy target.

The paper is organized as follows. The Doppler property of a BPSK signal coded with a maximum-length sequence (*m*-sequence) is reviewed in Sec. II to compare with other popular waveforms. Target echo is identified by delay and

Doppler. The active experiment is described in Sec. III, followed by data analysis. The reverberation amplitude statistics is studied in Sec. IV. One-way TL measurement and modeling are presented in Sec. V to assess the echo strength as a function of range. System implications are discussed in Sec. VI. A summary is given in Sec. VII.

## II. DOPPLER ANALYSIS: THE WAF

The purpose of active radar/sonar systems is not only to detect the echo buried in the noise/reverberation but also to estimate the range and velocity of the target, and distinguish the target echo from clutter to avoid false alarms. So the signals to be used must not only provide a sufficient processing gain to combat the noise but also exhibit a good time and frequency resolution. Under noise-limited detection conditions, detection performance can be improved by increasing the signal energy/duration, using, for example, pulsed continuous waves (CWs). Under reverberation-limited conditions (where reverberation level also increases with signal energy/duration), performance is dependent on both signal duration (*T*) and bandwidth (*B*), normally requiring wideband signals. The basic tool for performance characterization is the WAF originally used to analyze a given (transmitted) signal.<sup>10–12</sup> Here, we use a generalized WAF, which has been widely used in the literature to analyze the received data,<sup>13</sup> defined as

$$\Phi_r(\tau, \alpha) = \int_{-\infty}^{\infty} x_{\alpha}(t - \tau)r(t)dt = x_{\alpha}(-t) \otimes r(t), \quad (1)$$

where  $\otimes$  denotes the convolution operator,  $r(t)$  denotes the received signal, and  $x_{\alpha}(t) = \sqrt{\alpha}s(\alpha t)$  is the time compressed or dilated version of the transmitted signal  $s(t)$ , where  $\alpha$  is the compression/dilation ratio, referred as the Doppler ratio, and  $\tau$  denotes the delay time. Expressing the received signal by  $r(t) = h_{\alpha_0}(t) \otimes x_{\alpha_0}(t) + n(t)$ , where  $\alpha_0$  is the target Doppler ratio,  $h_{\alpha}$  is Doppler-adjusted active system impulse response, and  $n(t)$  denotes the ambient noise, one finds

$$\begin{aligned} \Phi_r(\tau, \alpha) &= h_{\alpha_0}(t) \otimes [x_{\alpha}(-t) \otimes x_{\alpha_0}(t)] \\ &\simeq \int_{-\infty}^{\infty} h_{\alpha_0}(t)\Phi_s(t - \tau, \alpha - \alpha_0)dt, \end{aligned} \quad (2)$$

where we have ignored the noise term assuming high signal-to-noise ratios. One sees that the Doppler and range resolution is determined predominantly by the WAF of the transmitted signal  $\Phi_s$ . The WAF of the received signal  $\Phi_r$  is a superposition of the WAFs of the transmitted signal delayed by the multipath arrival time and weighted by the multipath amplitude; the multipath Doppler is in general dependent on the path grazing angle.

For a given Doppler ratio, Eq. (1) can be viewed as a matched filter processor, or a correlation receiver, where  $x_{\alpha}(t)$ , referred to as the replica signal, is used to match (correlate) with the data. For a point target moving with a radial speed  $v$  toward the receiver, the Doppler ratio is given by  $\alpha \simeq 1 - 2(v/c)$ , where  $c$  is the reference sound speed. The delay time  $\tau$  is related to the target range  $r$  by  $r = \tau c/2$

approximately. For a narrow-band signal (i.e., bandwidth much smaller than the carrier frequency), the time compression/dilatation of the envelope function can be ignored, and the Doppler waveform is obtained by shifting the carrier frequency of the transmitted waveform. The corresponding ambiguity function, using Eq. (2), reduces to the well-known Woodward ambiguity function. See Refs. 10–12 for discussions on the differences between the two functions. One notes that in practice,  $v \ll c$ , hence the Doppler ratio is very close to 1. It is more intuitive to display the WAF in terms of the Doppler shift of the center (or carrier) frequency (Doppler frequency) given by  $\delta f_c = (1 - \alpha)f_c = 2(v/c)f_c$  as is done for a narrowband signal. This convention will be adopted in this paper.

The WAF is often used to study the resolution performance of the correlation receiver; the performance is generally dependent on the signal waveform used.<sup>5–12,14</sup> Analytical properties of the WAF (of the transmitted signal) have been studied in the literature for CW, LFM, HFM pulses,<sup>5,6,10–12</sup> and BPSK signals,<sup>7,8,14</sup> and need not be repeated here. For the purpose of this paper, it suffices to illustrate the differences in terms of numerical examples to show the advantages of using the BPSK signal coded with an  $m$ -sequence as the Doppler filter. The simulation is done using the following equations. The pulsed CW signal is given by  $x(t) = A(t)\sin(2\pi f_0 t)$ , the LFM signal is given by  $x(t) = A(t)\sin[2\pi(f_0 t + 1/2kt^2)]$ , and the HFM signal is given by  $x(t) = A(t)\sin[2\pi/\beta \log(1 + \beta f_0 t)]$  where  $A(t)$  is the signal envelope,  $f_0$  is the initial frequency,  $f_0 = f_c \pm B/2$ , and  $k$  and  $\beta$  are the frequency sweep rates.<sup>11</sup> The BPSK signal is given by  $x(t) = A(t)\sin\{2\pi[f_c t + b(t)]\}$ , where  $b(t)$  is a binary sequence of codes, each of duration  $1/B$ . We assumed zero Doppler for the input signal.

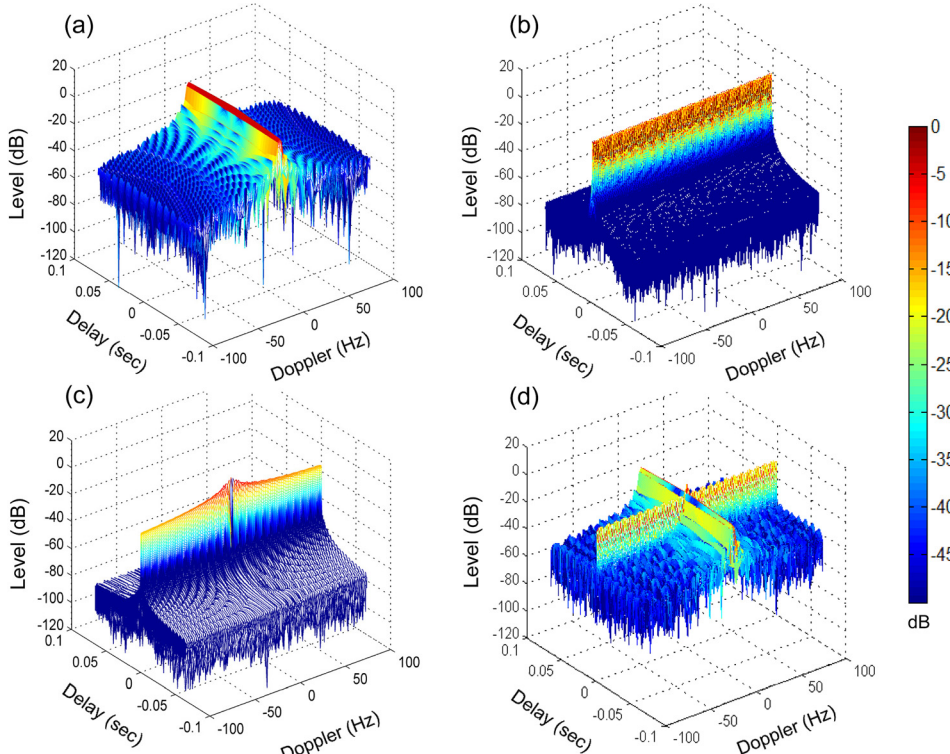


FIG. 1. (Color online) Wideband ambiguity surfaces for (a) CW, (b) HFM, (c) LFM, and (d) a combination of the CW + HFM pulses.

The WAFs of the above signals are displayed in Fig. 1 in terms of a two-dimensional surface as a function of the delay time and Doppler shift (of the center frequency), henceforth referred to as delay and Doppler in short. The width of the peak of the ambiguity surface reveals the resolution in delay and Doppler—the accuracy to which a target's range and radial speed can be estimated. Since the volume under the WAF is close to the square of the signal energy, it is conventional to plot the ambiguity function surface normalized by the signal energy. For the numerical examples, we use signal parameters corresponding to the experiment data analyzed in Sec. III. The CW, LFM, HFM, and BPSK pulses have a center frequency  $f_c = 50$  kHz, a duration  $T = 0.26$  s, and a bandwidth  $B = 15$  625 Hz except for the CW. A rectangular window is used. Figure 1(a) shows the ambiguity function for the pulsed CW. It has a high Doppler resolution, on the order of  $1/T$  but lacks range resolution as is well-known. The HFM signal has a high range resolution, on the order  $c/2B$ . It is known to be insensitive to Doppler; as seen in Fig. 1(b) the peak values of the ambiguity surface stay nearly flat across Doppler (within  $\sim 3$  dB). The ambiguity surface for the LFM signal, shown in Fig. 1(c), is similar to that of the HFM signal, except that its peak values at near zero delay-time drop by 16 dB from 0 to  $\pm 100$  Hz. It has a range resolution approximately the same as that of the HFM signal. The range resolution is sensitive to the Doppler at high bandwidth. As a result, low bandwidth LFM is often used for Doppler insensitive processing.

In active sonar, the CW and HFM pulses are often used in sequence. When there is only one target, one can determine the target range and speed using the HFM and CW waveforms separately. When there are more-than-one (strong) returns, it is difficult to determine the delay and Doppler of the target, since one cannot uniquely associate

the Doppler with the delay. An alternative is to transmit both the CW and HFM together. To determine how effective this approach is, one examines the ambiguity surface of the CW + HFM signal which is shown in Fig. 1(d). One finds that the target delay and Doppler is uniquely determined with a high resolution, based on the peak of the ambiguity surface shown in Fig. 1(d). But at the same time, one finds relatively high sidelobe levels in both delay and Doppler (approximately  $-6$  dB below the main peak). The high sidelobes could lead to an ambiguous or incorrect estimate of target delay and Doppler, when there are more-than-one scattered returns. For example, the ambiguity surface of two returns, shifted in delay and Doppler, will have four peaks in delay and Doppler. Where the sidelobes (from different returns) intersect, the addition (constructive interference) of the sidelobes could produce a higher peak than the main peaks. Even worse is the situation when the sidelobes from a strong object mask the echo return from a weak target, causing the target to be undetected.

Figure 2(a) shows the wideband ambiguity surface of the BPSK signal coded with an  $m$ -sequence of length 4095.<sup>15</sup> It shows a high peak centered at zero delay and Doppler, with low sidelobe levels in both delay and Doppler.<sup>16</sup> The peak-to-sidelobe ratio in delay is theoretically on the order  $10 \log(4095) \sim 36$  dB; the low sidelobe levels in delay are due to the cyclic orthogonality of the  $m$ -sequence. Figure 2(b) shows the color display (in dB) of the ambiguity surface where one zooms in on the peak. It shows more clearly the delay and Doppler resolution. Near the peak, the ambiguity function can be approximated by  $\Lambda(\tau B)\text{sinc}(\pi\Delta T)$ , where  $B$  and  $T$  are the signal bandwidth and duration as defined above,  $\Lambda$  is the triangular function, and  $\Delta$  denotes the Doppler shift.<sup>7,14</sup> The triangular and sinc function dependence is observed in Fig. 2(b). There is no coupling between delay and Doppler. The delay resolution measured at  $-3$  dB point is  $\sim 0.04$  ms, corresponding to a range resolution of  $\sim 0.03$  m.

The Doppler resolution measured at  $-3$  dB point is  $\sim 2.5$  Hz. Such fine resolution is the result of the large bandwidth and long duration of the signal for the purpose of boosting the processing gain and suppressing the sidelobe levels.

{The fine range resolution turns out to be a disadvantage in target search in real data using a color display as discussed below, since the sharp peak is only observable when one zooms in on the peak due to the limited number of pixels in the color display. This is confirmed here using simulated data, for which signal distortion by the propagation channel is not an issue. One finds indeed that the peak is not observable if the color display uses a time window equal or greater than  $\pm 50$  ms, corresponding to a range span of 75 m [Fig. 2(b)]. For initial target detection/location over a wide range, one can use the mesh display of the ambiguity surface as shown in Fig. 2(a).}

Figure 2 shows an evenly distributed low sidelobe level in delay and Doppler with practically no coupling between delay and Doppler. This presents a significant advantage for active sonar, when multiple high-level discrete returns are present in the data, since target and clutter can be identified by Doppler, and leakage between the two (due to sidelobes) is not a problem. Assuming that clutter originates mostly from fixed or slowly moving objects, it is expected to have a small Doppler shift. As such, clutter can be removed by Doppler processing to improve the signal-to-reverberation ratio. Since delay and Doppler are determined for each high level return, target range and speed will not be confused with that of the clutter and can be estimated accurately. These advantages will be demonstrated using real data in Sec. III.

In terms of data processing, HFM and CW pulses are often the favorite waveforms, since one HFM replica can be used for targets of practically any speed, and the replica receiver for the CW pulse can be implemented efficiently with a fast Fourier transform. For the BPSK signal coded with an

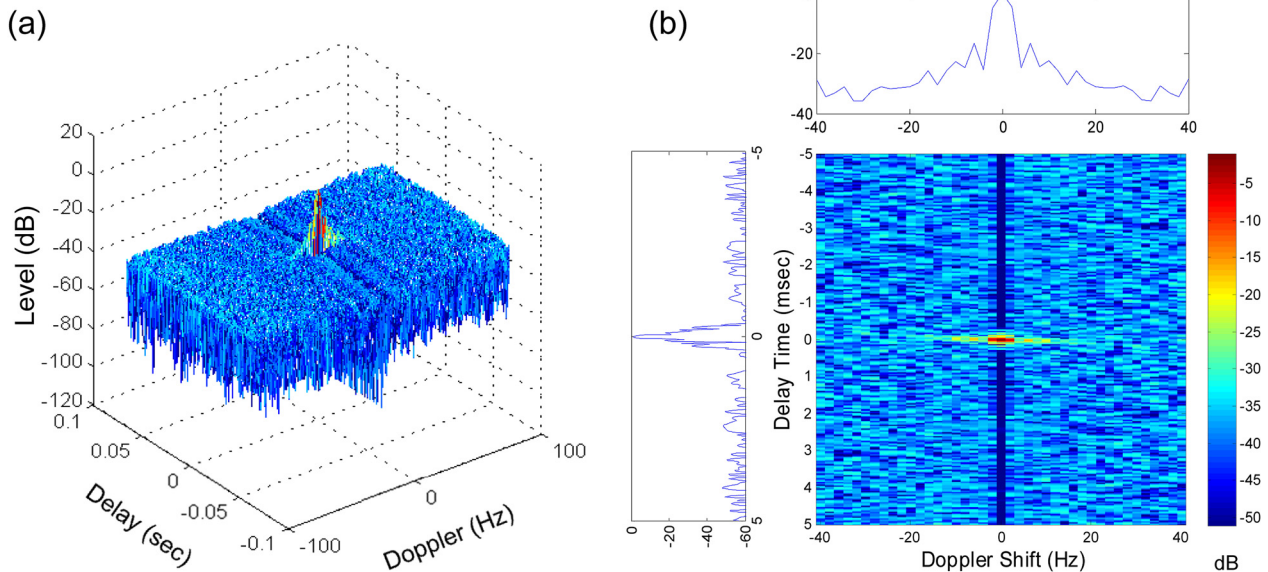


FIG. 2. (Color online) Wideband ambiguity surface for a BPSK signal coded with an  $m$ -sequence. (a) A 3D mesh plot. (b) A color plot zooming on the main lobe.

*m*-sequence (referred to as an *m*-sequence signal in short), the WAF is calculated in the baseband. The data are first demodulated into baseband and down sampled to a rate equal to twice the signal bandwidth. The signal replica is calculated at discrete Doppler shifts to match with the data.

### III. ACTIVE EXPERIMENT AND DATA ANALYSIS

An experiment was conducted in the Woods Hole Harbor in August 2009 to study the active returns using both Doppler insensitive and sensitive waveforms.<sup>17</sup> A 32 in. air-filled steel sphere with a weight at the bottom (supported by another 32 in. sphere at the surface) was towed approximately 10 m behind a ship moving with a speed of 3 to 4 knots, at a depth of an estimated 3 to 6 m, to emulate a moving target. A directional source with a beam width of 6° and a directional receiver with a beam width of 16° were deployed at the pier at a depth of ~9 m pointing to the target as shown in Fig. 3. The source and receiver are spaced horizontally at a distance of ~13 m forming a “mono”-static active system. The Woods Hole Harbor has an average depth of 12 m along the tracks. At some spots, the water depth can be as shallow as 9 m and as deep as 15 m.

LFM pulses and the Doppler sensitive *m*-sequence signals centered at 50 kHz were transmitted in sequence, and repeated one after the other, so that both signals encounter the same propagation and reverberation conditions. The signals were separated by a sufficient time (~1 s) to allow target

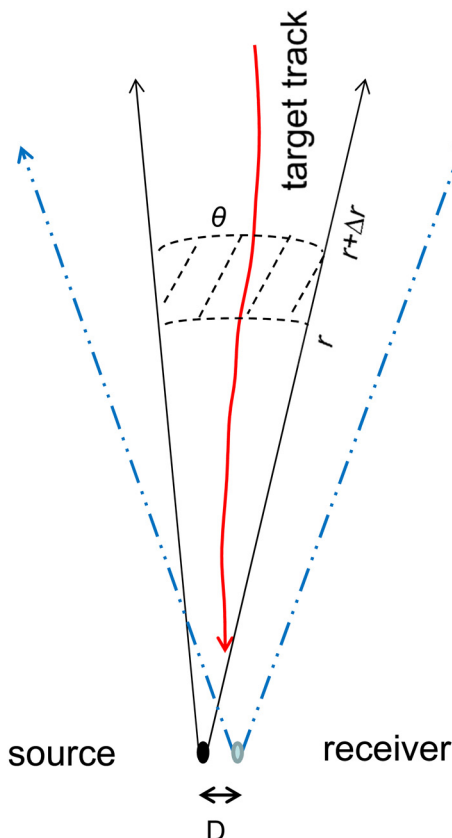


FIG. 3. (Color online) Top view of the target track relative to the directional source and receiver. The area covered by the dashed lines is ensonified by the source at a delay time  $\tau = 2r/c$ .

detection up to a range of 750 m and reverberation to recede to the noise level. The LFM signal has a bandwidth of 10 000 Hz and duration of 0.1 s. The BPSK signal has a bandwidth of 15 625 Hz and duration of 0.26 s. Both signals have approximately the same total energy during transmissions.<sup>18</sup> (The bandwidth dependence is discussed in Sec. IV.) The purpose of this paper is to evaluate the capability of the Doppler sonar to discriminate or separate the target echo from reverberation. The matched filtered outputs based on the LFM signals are used to assess the echo and reverberation level and arrival time to serve as a reference for comparison.

#### A. The LFM data

Ideally, to study the acoustic properties of the target echo and reverberation, one should transmit a high level impulse signal to get the “ground truth” of the active returns. In practice, such a high-level impulse source is often not available, and one spreads the signal (energy) over time and uses matched filtering to compress the received signal to obtain the equivalent of the ground-truth signal. For moving objects, one should use Doppler insensitive waveforms for this purpose, for which we chose the LFM signal. Figure 4 shows the matched filtered outputs of the received time series (using the LFM waveform) as a function of delay time for 79 pings; the y-axis displays the ping transmission (geotime) time. Zero Doppler-shift is assumed here for the replica since the result is not sensitive to the Doppler. The target echo is highlighted and indicated by “target” in Fig. 4 (based on the GPS target range) visible to a round trip delay time of ~0.35 s, or range of 225 m, assuming  $c = 1500$  m/s. One also finds in Fig. 4 many high-level backscattered returns covering an extended range of delay time, with levels sometimes higher than the target echo. In addition to the target line showing a relatively high radial-speed target moving toward the sonar, there exist other potential tracks, as indicated by concentrations of energy forming a near-vertical broad track showing relatively small radial-speed (based on their range rate), which could be falsely identified as targets (swimmers) by a novice observer. The origin of these high level returns will be analyzed in Sec. III B using the Doppler analysis. One finds that these non-target returns are likely backscattered returns from objects (debris/fish/shrimp) in the water column, moving with a slow speed, away from the source. They will be referred to as volume reverberation in this paper.

The data suggest that target detection and classification (recognition) may be hindered by the high-level reverberation without first tracking the target to eliminate the clutter outside the target range cells. Figure 5 shows the time series of eight pings evenly spaced in time, when the target is close and has a high signal level. One sees that the time series show many high level peaks; which one is the target is ambiguous. As a result, the target range cannot be reliably estimated. Whether the target has a high speed (and poses immediate danger) cannot be determined based on (just) eight pings of data. Hence, one must rely on the target track analysis based on the target kinematics, which can be done, in principle, with just a few pings but, in practice, likely

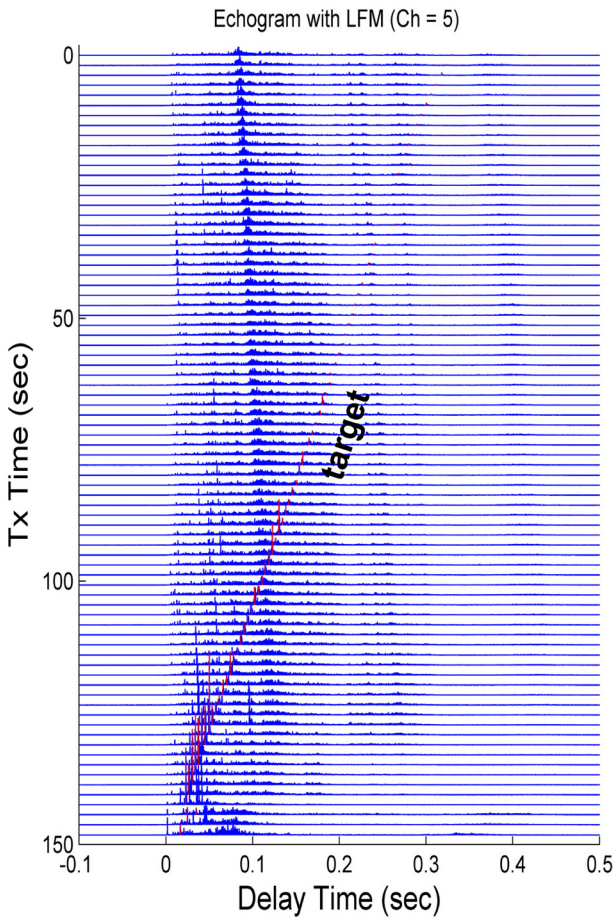


FIG. 4. (Color online) Matched filtered output as a function of the delay time for each LFM ping, stacked over many pings. Vertical axis denotes the ping transmission (Tx) time. Amplitude in arbitrary units but fixed between the different pings.

requires many pings to reduce the uncertainty. Thus, we explore alternative means of target discrimination using the Doppler as the discriminator as done in airborne radar. In airborne radar, detection is based mostly on the direct path; ground clutter are known and well separated in time from the target. The target return has a high signal-to-noise/rever-

beration ratio and its Doppler can be measured with sufficient precision using narrowband signals. The problem in underwater Doppler is much more difficult. One deals with multipath returns including continuous as well as discrete reverberation returns. The target signal-to-noise/reverberation ratio is generally low. To improve discrimination against reverberation, one needs to use broadband signals as discussed above. How well the Doppler discrimination works is the subject of Sec. III B.

## B. The *m*-sequence data

Doppler discrimination is based on the WAF as discussed in Sec. II. Doppler processing is done by matched filtering the raw data with Doppler compensated *m*-sequence signals. This requires in the baseband not only phase correction due to Doppler shift of the carrier frequency but also time compression/dilation of the signal envelope. For target detection and localization, one searches the ambiguity surfaces over a wide range of delay and Doppler based on possible target ranges and speeds. The peak of the ambiguity surface is used to estimate the target delay and Doppler as well as the target impulse response.

In this section, we examine the delay and Doppler resolution based on data where the target has been detected/localized. Using received data from a signal transmitted at Tx Time = 97.8 s as an example, the ambiguity surface in the neighborhood of the target echo is shown in Fig. 6(a), and is used to illustrate the data processing leading to the Dopplergram and Doppler filtered time series (presented in Secs. III B 1 and III B 2 below). Figure 6(a) shows a sharp peak with >25 dB peak-to-sidelobe ratio at a delay time of ~0.129 s and Doppler frequency of ~100 Hz, indicating the presence of a target moving with a radial speed of 3 knots, located at a range of ~97 m from the source/receiver. Plotting the ambiguity function at a fixed delay time of ~0.129 s (the delay time of the peak) as a function of the Doppler frequency, one obtains the target ambiguity function as a function of the Doppler shift (referred to as the *Doppler spectrum*) as shown in Fig. 6(b). Plotting the ambiguity

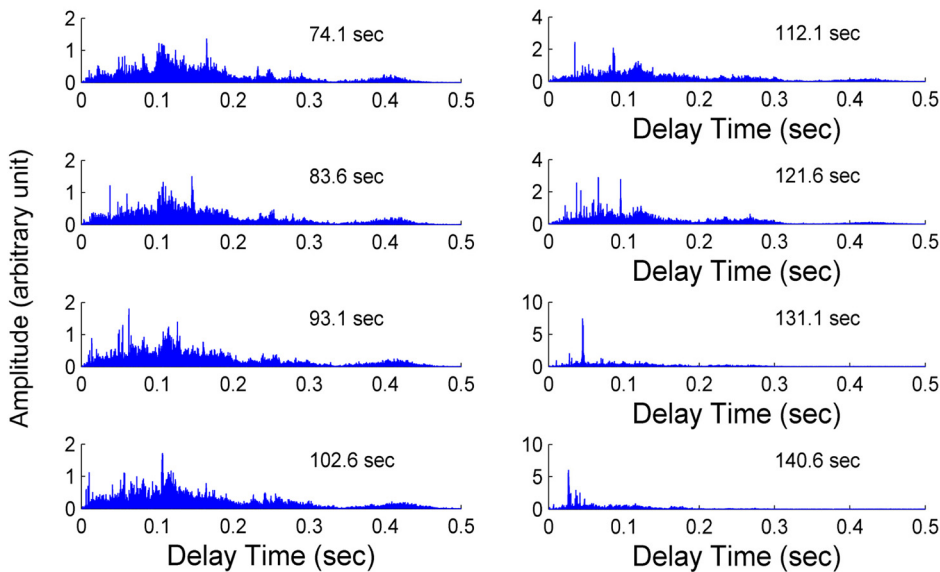


FIG. 5. (Color online) Expanded view of the matched filtered outputs as a function of the delay time for selected LFM pings.

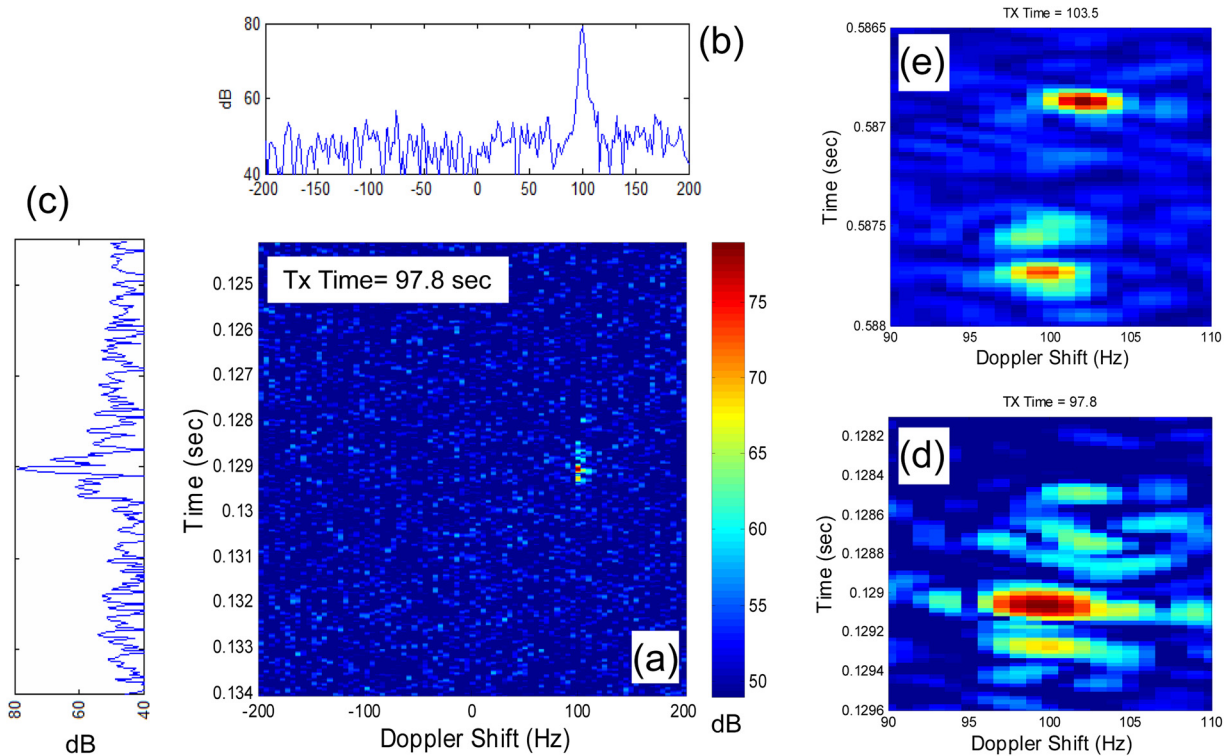


FIG. 6. (Color online) (a) Wideband ambiguity surface as a function of delay time and Doppler shift based on data transmitted at Tx time of 97.8 s. (b) Target ambiguity function as a function of Doppler shift. (c) Reverberation time series evaluated at a Doppler shift of 100 Hz showing the target echo. (d) A zoom in display of the ambiguity surface showing the target impulse response at Tx time of 97.8 s. (e) Another example of the target impulse response at Tx time of 103.5 s. (d) and (e) follow the same color scale as in (a).

function at a fixed Doppler shift of  $\sim 100$  Hz (the Doppler shift of the peak) as a function of the delay time, one obtains the *echo time series* as shown in Fig. 6(c). It is the matched filtered output as a function of the delay time assuming a Doppler shift of 100 Hz. The Doppler Spectrum and echo time series are saved for each ping to create the Dopplergram and Doppler-filtered time series.

To examine the Doppler and temporal (or equivalently range) resolution, one zooms in on the impulse response as shown in Fig. 6(d) for the signal as Tx Time = 97.8 s.

Also shown in Fig. 6(e) is another example of the impulse response at TX time = 103.5 s. One finds 3 to 4 multipath returns, having sometimes different Doppler shifts with respect to the carrier frequency (by 2 to 3 Hz). Figures 6(d) and 6(e) show that the ambiguity surface has a temporal resolution of  $\leq 1$  ms, yielding a range resolution of  $\leq 1$  m. However, range estimation has some uncertainties due to multipaths, synchronization error, and clock inaccuracy which could exceed 1 ms. One finds the ambiguity surface has a Doppler resolution of 2 to 3 Hz, consistent with the simulation result shown in Sec. II. The peak to average side-lobe level is about 30 dB, compared with the theoretical value of  $\sim 36$  dB. The processing gain in the real world is expected to be less than the theoretical value due to high reverberation returns (which increase the background level), and limited channel coherence time, leading to a decrease in the matched filter gain.

Without knowing/presuming the existence of a target, one searches blindly the peak(s) of the ambiguity surface

for each ping. The Doppler spectra are stacked as a function of time to form a Dopplergram as discussed below. The echo time series are stacked together to estimate the target track.

### 1. Dopplergram

Repeating the Doppler processing for each ping, and stacking the *Doppler spectra* [Fig. 6(b)] from the peak(s) of the ambiguity surface over the transmission time, one obtains a Doppler spectral gram (referred to as the Dopplergram<sup>9</sup>) as shown in Fig. 7. Two Doppler frequency lines are noted in Fig. 7. They are, generally speaking, not associated with the same target, more likely with different “targets” at different ranges (different arrival time). The purpose of the Dopplergram is to determine potential targets in the Doppler space, without initially localizing/tracking them in range. In doing so, one uses the Doppler frequency/spectra to discriminate the targets from the reverberation.

One finds two tracks in the Doppler space in Fig. 7. One, denoted by A, is concentrated at 100 Hz, decreasing to 75 Hz near the end, and the other, denoted by B, stays between  $-20$  and 0 Hz. Dopplergram follows the same concept as Lofargram used in passive sonar. In passive narrowband detection, given a snapshot spectrum, there are likely many spectral peaks that are not associated with the target. Given a continuous record (Lofargram), target detection is improved since target spectral lines are continuous with time, whereas the spurious lines are usually not. The same concept is adopted

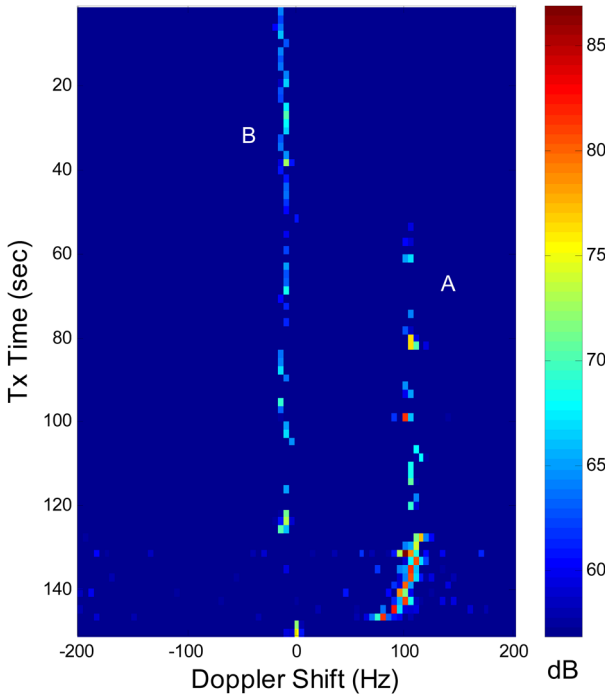


FIG. 7. (Color online) Dopplergram of the active sonar returns.

for a Dopplergram. The Dopplergram (Fig. 7) suggests two (or more) potential moving targets (based on the aggregation of data points around two bands of Doppler frequencies): One with a high Doppler shift or high radial speed, and the other with a low Doppler shift, or low radial speed. The high Dopp-

ler returns have much higher intensities than the low Doppler returns, suggesting higher target strengths. The Dopplergram can be used to track a moving object through the closet point of approach as discussed in Ref. 9.

For this experiment, one knows that there is no target moving with a small radial-speed. The low Doppler returns must be some kind of reverberation returns. The origin of this low Doppler return is discussed in Sec. III B 2.

## 2. Doppler filter

Airborne radar uses a Doppler filter to pass the desired signals (to subsequent processing) and reject the unwanted signals based on their Doppler content. Since the signal bandwidth is much smaller than the carrier frequency in airborne radar, the Doppler filter is basically a narrowband filter. For wideband signals as in Doppler sonar, one uses a high-pass filter for fast moving targets, and a low-pass filter for slowly moving reverberation. For the data analyzed above, having identified potential moving targets in the Doppler space, one can narrow the target search to two Doppler bands, i.e.,  $-20$  to  $0$  Hz and  $60$  to  $120$  Hz. Searching the ambiguity surface in the  $60$  to  $120$  Hz band by restricting the Doppler replica in this band (or high-pass at  $60$  Hz), one obtains the echo time series associated with the peak of the ambiguity surface from each ping. They are stacked over the transmission time and plotted as a function of delay time as shown in Fig. 8(a). Figure 8(a) is to be compared with the similar time series using the LFM signal as shown in Fig. 4. One sees that the high-level reverberation returns seen in

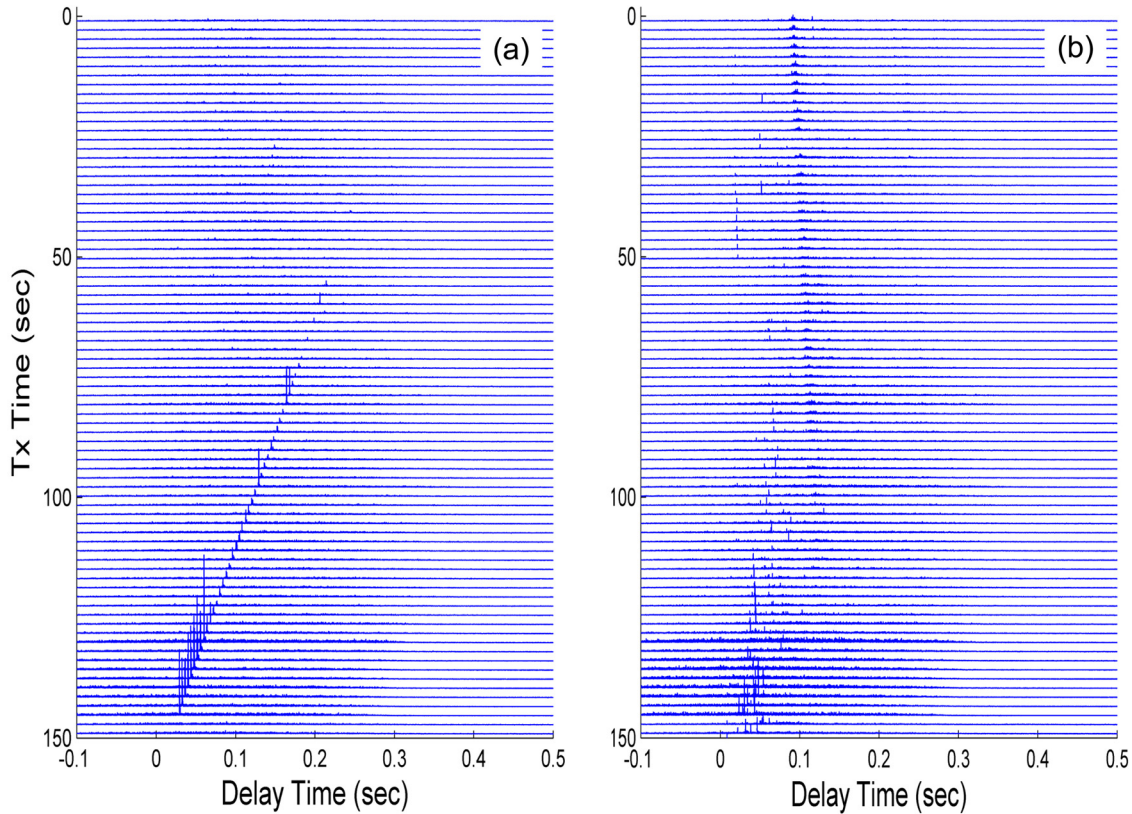


FIG. 8. (Color online) Doppler filtered time series focused on the target Doppler (a) and low band Doppler (b) using the  $m$ -sequence data, stacked over many pings. Amplitude in arbitrary units but fixed between the different pings.

Fig. 4 are absent in Fig. 8(a); these returns have been removed by the Doppler processing.

Applying the same processing to the low Doppler band between –20 and 0 Hz, the echo time series of the ambiguity surfaces for each ping are plotted as a function of the delay and stacked over the transmission time as shown in Fig. 8(b). One finds that the low Doppler returns show a similar arrival pattern (with the same slopes) and can be identified as the “same” reverberation returns seen in Fig. 4.

What could be the origin of these negative Doppler returns? (None such returns were reported in published literature to our knowledge.) Possible sources that can contribute to the low Doppler backscattered returns are rough sea surfaces and wave generated bubbles, wakes generated by the tow ship, ocean currents, etc. Upon further examination, one finds that the reverberation could not come from the surface waves as the sea is relatively smooth based on visual observation during the experiment. Small sea surface ripples (at the scale of the acoustic wavelength) are expected to be random and isotropic in the absence of directional waves. For this scenario, one expects that the backscattered returns from the surface waves should have a Doppler shift with a mean centered at zero Doppler. Second, the reverberation could not have come from the ship wakes (and bubbles generated by the ship) since the reverberation level did not increase as the ship gets close to the source/receiver. Third, one observes that reverberation is much more diffused in non-target than target directions (based on data collected on receivers pointing at other directions, which are not discussed in this paper). This suggests that the scatterers are moving more or less in one direction (target look direction) away from the sonar. The most likely source for the scattered returns is debris/fish/shrimp flowing with the ocean tidal current. In the post analysis, we found some Acoustic Doppler Current Profiler (ADCP) data collected in a nearby island (Martha’s vineyard) which measured the tidal current around the experiment time, showing that the experiment took place at about 2 h after the high tide. The current speed measured by ADCP was 0.1 to 0.2 m/s, which is consistent with a Doppler shift of about 10 to 20 Hz found in the data. We thus hypothesize that the low Doppler returns are backscattered returns from volume inhomogeneities or volume reverberation in short.

One notes that there are less numbers of high-level (low-Doppler) reverberation returns in the echo time series in Fig. 8(b) than there are in the (volume) reverberation returns in Fig. 4 (for a given threshold). This is due to the fact that Fig. 8(b) only plots the echo time series associated with the (highest) peak of each ambiguity surface. In principle, if the low Doppler returns are volume reverberation, they will likely show up as multiple peaks in the ambiguity surfaces. To reproduce the high-level volume reverberation returns, one needs to estimate and combine the echo time series from the multiple peaks, which is not done here.

Note that noise is insensitive to Doppler processing; in other words, it appears with more or less uniform levels irrespective of the Doppler frequency. So are incoherent background reverberations coming from randomly distrib-

uted scatterers. They are not suppressed or discriminated by Doppler processing.

#### IV. REVERBERATION ENVELOPE STATISTICS

The amplitude statistics of the reverberation (also known as the matched filtered envelope statistics) are relatively unexplored at high frequencies, and, in particular, in a harbor environment to our knowledge. In this section we investigate the amplitude statistics of the high-level volume reverberation using the LFM data (treating the matched filtered outputs as the “true” reverberation time series). In comparison, we will investigate the statistics of the background reverberation after applying the Doppler filter to the *m*-sequence data.

In general, the amplitude of the reverberation is expected to be Rayleigh distributed if the reverberation is comprised of backscattered returns from enough scatterers in a given cell so that the central limit theorem (CLT) holds or when the scatterer’s density and sizes follow a Gaussian distribution. The distribution could become non-Rayleigh as sonar beam resolution improves due to the number of scatterers ensonified becoming small and thus voiding the CLT, or when the scatterers within the small cell do not follow the Gaussian distribution. In these cases, the distribution normally has a heavy-tail due to high level returns from certain highlighted objects. Against this background, one is interested to know the nature of the amplitude statistics of the high-level volume reverberation found in this experiment. To determine that, we take 468 samples (each 2 ms long) from the matched filtered output of each LFM ping at a delay time of 0.1 s, excluding those samples when the target is present (see Fig. 4). The data samples are combined to calculate the amplitude distribution. The result is shown by the dashed line in Fig. 9(a). One finds that it has a non-Rayleigh distribution.

We next investigate the amplitude distribution of the residue reverberation after applying the Doppler processing. We apply the same analysis to the Doppler filtered echo time series in Fig. 8(a) at a delay time of 0.1 s, excluding the data samples when target is present. The result is shown in Fig. 9(a) by the solid line marked by the plus sign; it is reasonably well fitted by a Rayleigh distribution. Alternatively, one can evaluate the reverberation statistics using the Dopplergram (Fig. 7) by taking samples 30 to 50 Hz away from the target Doppler over all transmission time. One finds that this method yields a similar distribution as the above method (the result not shown here). [We note that the *m*-sequence data has ~56% more bandwidth than the LFM data. To study the bandwidth dependence, we apply a bandpass filter to the time series in Fig. 8(a), limiting the bandwidth to 10 kHz and renormalize the time series to have the same variance as that before the filter. The result is shown in Fig. 9(a) by the solid line. It has basically the same distribution as that found from the original (Doppler filtered) time series, i.e., the solid line marked by the plus sign.] Using the first method, one finds that while the distributions of the amplitudes remain Rayleigh-like at “all” delay times, the mean amplitude of the residue reverberation varies with the delay time since the

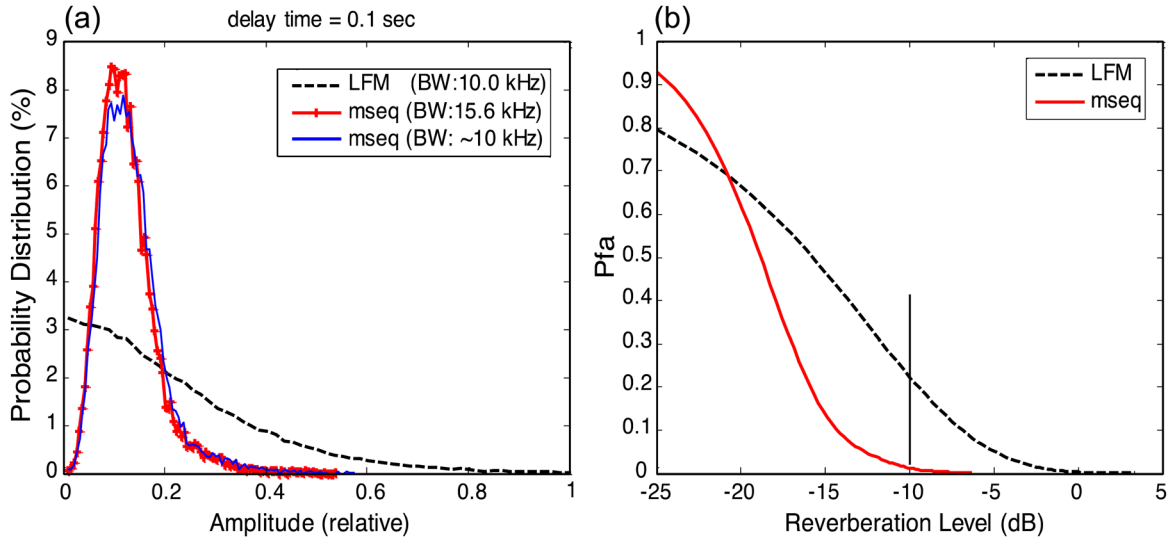


FIG. 9. (Color online) (a) Probability distribution of the reverberation amplitude sampled at a delay time of 0.1 s. The LFM data (dashed line) show a non-Rayleigh distribution whereas the Doppler-filtered residue reverberation, shown by the solid line marked with +, follows a Rayleigh-like distribution. The solid line shows the Doppler-filtered residue reverberation with a smaller bandwidth. (b) The corresponding  $P_{fa}$  as a function of the reverberation level.

total reverberation is a function of the delay time (or range). Using the second method, one finds that the amplitude distribution is insensitive to the Doppler frequencies of the samples, as long as they are sufficiently separated from the high level (target and/or volume reverberation) returns.

The mean intensity of the residue reverberation is approximately 6 dB lower than that of the unfiltered reverberation (the matched filtered envelope of the LFM data) using data presented in Fig. 9(a). This difference in reverberation level is reflected in a lower  $P_{fa}$  as discussed in Sec. VI.

## V. TARGET ECHO AND MODELING

Another element that enters the sonar equation is the target echo level, which depends on the target strength as well as the two-way TL. Barring sharp angle dependence of the target strength, the decrease of the echo level as the target range increases is determined predominantly by the two-way TL. To develop a modeling capability, we conducted the one-way TL measurements during the experiments by

deploying a hydrophone 1 ft. above the target. The range to the source is determined from the towing ship GPS data. Figures 10(b) and 10(c) show the received signal level (RL) as a function of range for various tow runs as shown in Fig. 10(a). One finds that the received signal level (correspondingly the TL) varies significantly (10 to 30 dB) between runs. This suggests that the bathymetry has a significant influence on high frequency sound propagation.

For a given run, large signal fluctuations can be a result of signal fading at locations (shadow zones) where rays do not reach as a result of using directional sonar with a narrow vertical beam. If so, a more sophisticated sonar design will be required. Whether shadow zone exists or not is investigated below by modeling the TL using ray tracing. Large signal fluctuations can also be caused by constructive or destructive interference between multipath arrivals. Such phenomena should be reproducible using a coherent propagation model. For reference (benchmark) purposes, one likes to know: How much signal fluctuation does a (coherent) ray tracing model predict assuming a flat bottom? If the model

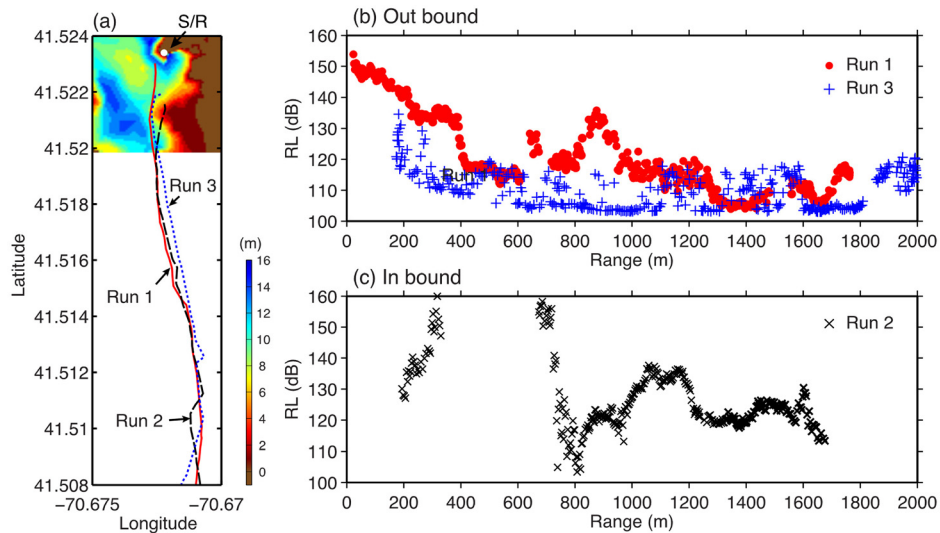


FIG. 10. (Color online) Received signal level (RL) as a function of range for: Two out-bound runs (b) and one in-bound run (c). The ship tracks are shown on the left (a) together with bathymetry in the inner harbor (bottom depth in meter). The ship tracks for Runs 1 to 3 are indicated by solid, dotted, and dashed lines, respectively. The source/receiver (S/R) position is indicated by an arrow, marked by a white dot.

fails to match the observed signal fluctuation, can it match the mean TL? From a system design perspective, one would like to know: How detailed a bathymetry is needed to predict/model the TL and how much of the sound fluctuation is not due to the bathymetry but due to the sound speed fluctuation in the ocean media. While these questions have been studied extensively at low frequencies, little is known at high frequencies, nor can we answer these questions without detailed environmental measurements; detailed bathymetry and sound speed profiles were not available during the experiment. In this section we limit ourselves to two basic questions: How much shadowing would directional sonar produce for a more or less flat bottom, and can the mean signal level data be reasonably modeled?

To model TL, we map out the bottom depth along the ship tracks using the bathymetry chart for the inner harbor [see the color plot in Fig. 10(a)]. For run 2, one finds that the propagation path [dashed line in Fig. 10(a)] encounters a “seamount” which rises  $\sim 10$  m above the bottom in a water of average depth of 12 m. The relatively large variation of the received level [Fig. 10(c)] may be related to the upslope enhancement and downslope spread of the signal over the seamount. For run 1, the bottom bathymetry is shown in Fig. 10(a) up to the 400 m range; beyond that the bottom is assumed flat for lack of data. Since the bathymetry along run 2 is not known in detail, we shall concentrate on run 1. For the TL calculation in a range dependent environment with a directional source, we use the Bellhop ray tracing program.<sup>19</sup> The source is located at a depth of 9 m, with an initial ray launch angle limited to  $\pm 6^\circ$  from the horizontal direction. We assumed a constant sound speed profile of 1500 m/s, which is a reasonable assumption for shallow depths. Figure 11(a) shows the modeled TL as a function of range averaged over a receiver depth between 5 and 6 m. The TL data is determined from the RL data by adjusting the source level until the mean (range averaged) TL data is in good agreement with the modeled TL, as shown in Fig. 11(a). One observes that the modeled TL does not reproduce the range

variation of the TL data within ranges between 400 and 1000 m, where the bottom bathymetry is not known.

Using the modeled TL, one can model the target echo level as a function of target range since the target echo level is the source level minus twice the TL plus the target strength, all in dB, treating the target strength as a constant (noting that the scattering function for the sphere is angle independent). The modeled echo level is fitted to the measured echo level data as shown in Fig. 11(b) by adjusting the target strength (having determined the source level above). The modeled echo level can be interpreted as the mean echo level as a function of range ignoring the dependence of the TL on the bathymetry and could be used for system performance analysis.

## VI. SYSTEM IMPLICATIONS

To model the detection performance, one needs to know the target strength and echo amplitude statistics. The former is not measured, although one can estimate it theoretically based on the manufacturer’s specification. The latter (statistical distribution) requires a large amount of data which we do not have. While the system performance is beyond the scope of this paper, some implications can be drawn based on the data presented above (see below).

### A. Normalized reverberation time series

The active sonar return is often processed/displayed in terms of the so-called normalized reverberation time series. In this processing, one cross-correlates the replica with sliding windows of data, with length equal to the replica, and normalizes the results by the square-root of the energy of the sliding windows of data.<sup>20</sup> If the replica is already normalized to have unit energy, then the maximum of the correlation is unity. This processing can be used to suppress the background reverberation which is random in nature, since the normalized cross-correlation of the replica with a random set of data is near zero. On the other hand, discrete or target-like returns are expected to have high cross-correlations. The high value reverberation returns in the normalized time series (that are not targeted related) are generally referred to as clutter.

The normalized reverberation time series for the LFM signal is shown in Fig. 12. One observes high level clutter returns not only at a delay time around 0.1 s as seen in the matched filter output (Fig. 4), but also at a delay time around 0.25, 0.3, and 0.45 s. These additional clutter returns have the same slope (in transmission time versus delay time) as the one observed before (at a delay time near 0.1 s), suggesting that they are volume scattered returns of similar nature. Why they are spaced more or less equally in range is not understood. In low frequency active sonar, as the sonar beam narrows, one expects that the amplitude distribution is heavy tailed but more or less evenly distributed in range. For this data, the high level reverberation (clutter) returns are not spatially stationary (homogeneous).

One can study the reverberation (clutter) amplitude statistics using the normalized reverberation returns. For comparison with the matched filtered outputs, one evaluates the amplitude

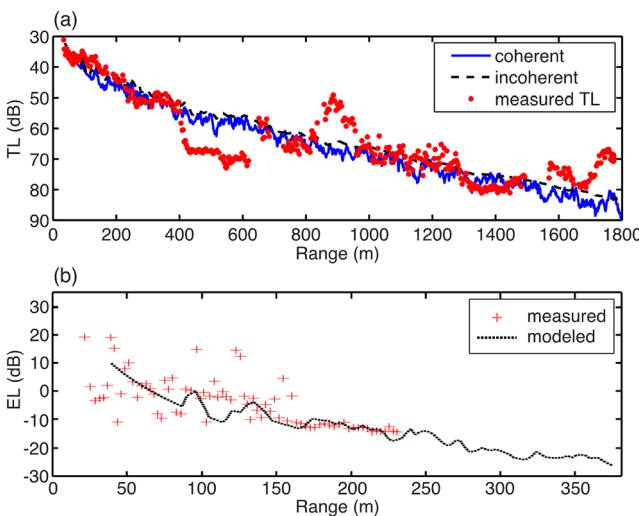


FIG. 11. (Color online) (a) Comparison of the modeled TL with the measured TL for run 1 of Fig. 10. (b) Target echo level data (marked by “+”) fitted with the modeled echo level.

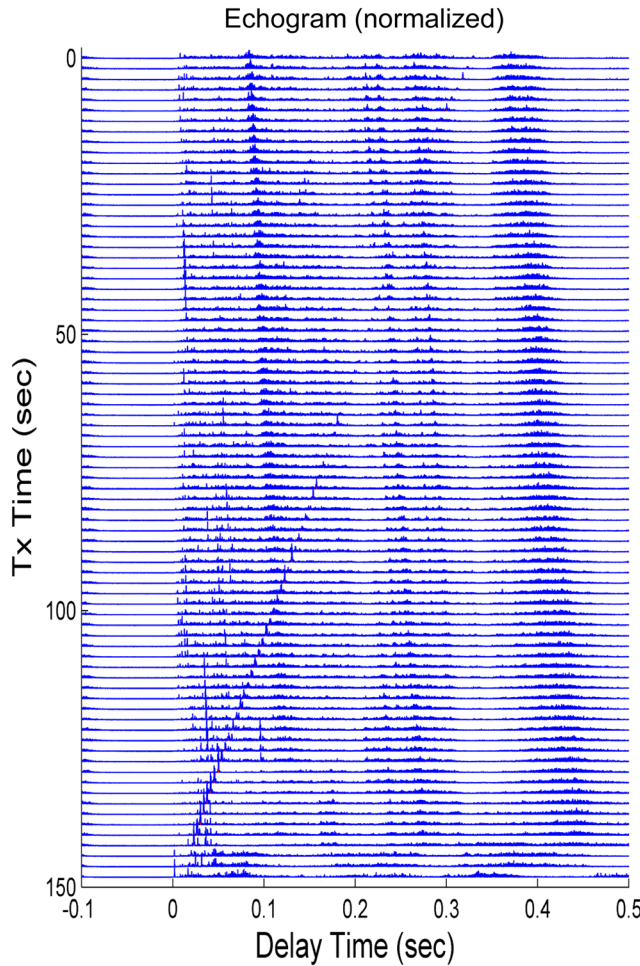


FIG. 12. (Color online) Normalized reverberation time series using the LFM signals. Vertical axis denotes the ping transmission (Tx) time. Amplitude in arbitrary units but fixed between the different pings.

distribution for the clutter return at  $\sim 0.1$  s delay. One finds that the amplitude statistics of the normalized returns have almost an identical distribution as that determined from the matched filtered output, i.e., the dashed line (LFM data) in Fig. 9(a), except that the amplitude is scaled down by a factor of  $\sim 10$ . This suggests that the reverberation (clutter) returns at  $\sim 0.1$  s are from discrete scatterers rather than random spatially distributed objects. (Conversely, if the random continuous reverberation returns were non-negligible in the unnormalized data but are mostly absent in the normalized data then their amplitude statistics, normalized vs unnormalized, will be significantly different.) For data that are clutter dominated (e.g., at delay time around 0.05, 0.1, 0.25, 0.3, and 0.45 s) normalization does not seem to (significantly) improve the signal-to-reverberation ratio. For data that are not clutter dominated, normalization can be expected to improve the signal-to-reverberation ratio. One observes that the target is tracked at longer ranges (round trip delay time  $> 0.25$  s) in the normalized display (Fig. 12) than in the unnormalized display (Fig. 4).

For the  $m$ -sequence data, since it is almost reverberation free, normalization does not show a dramatic effect except in leveling the background reverberation level to a near constant. The signal to reverberation level remains practically unchanged.

Note that the matched filtered outputs (the unnormalized data) display the signal versus the reverberation energy whereas the normalized data display the coherence (correlation) of the signal versus that of the reverberation (with respect to the transmitted signal). Since the focus of this paper is on acoustic properties of the signal and reverberation, we will discuss, for the remainder of this paper, the implication of the data for the energy detector using the matched filtered outputs. Using the constant false alarm rate (CFAR) detector, one determines the threshold level for a given false alarm rate. Based on the probability distribution of the reverberation for the LFM and  $m$ -sequence data [Fig. 9(a)], one estimates the corresponding Pfa as a function of the reverberation level, shown in Fig. 9(b). One finds that for a threshold level at  $-10$  dB, for example, the Doppler filtered reverberation ( $m$ -sequence data) shows a Pfa of  $< 0.01$ , whereas without Doppler discrimination, the LFM data shows a Pfa  $> 0.2$ . [The Pfa is the (integrated) probability that the reverberation amplitude is higher than the threshold, known as the complementary cumulative distribution function.] Conversely, for the LFM signal, in order to achieve Pfa  $\sim 0.01$ , one needs to raise the threshold level to  $-2$  dB (or higher). For Pfa  $\sim 0.01$ , the threshold level for the CFAR detector differs by 8 dB with and without the Doppler filter.

## B. Echo and peak-reverberation levels

The measured target echo levels are shown in Figs. 13(a) and 13(b) as a function of delay time (data points marked by “+”) for the LFM and  $m$ -sequence signals, respectively.

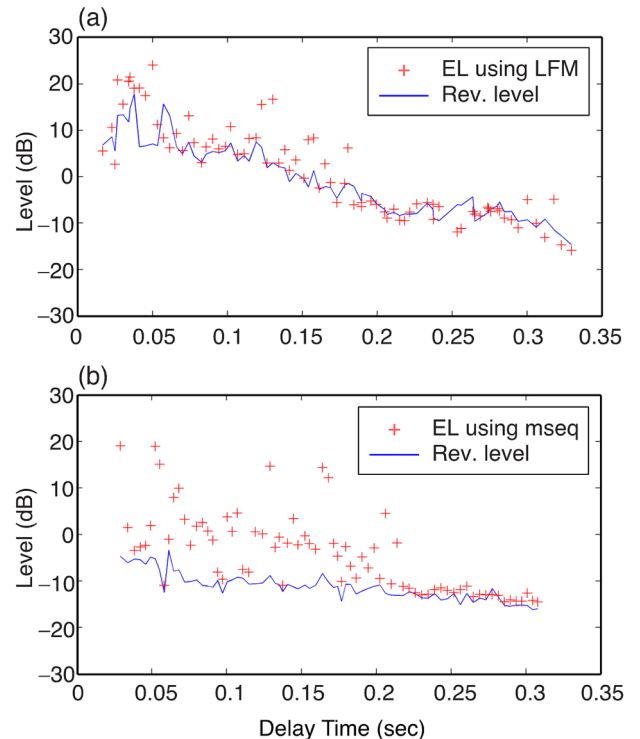


FIG. 13. (Color online) Target echo level (marked by “+”) compared with the peak level of the reverberation time series within 25 ms of the target signal (the solid line). Levels are estimated from individual ping data and displayed as a function of two-way travel time to the target (delay time): (a) The LFM data and (b) the  $m$ -sequence data.

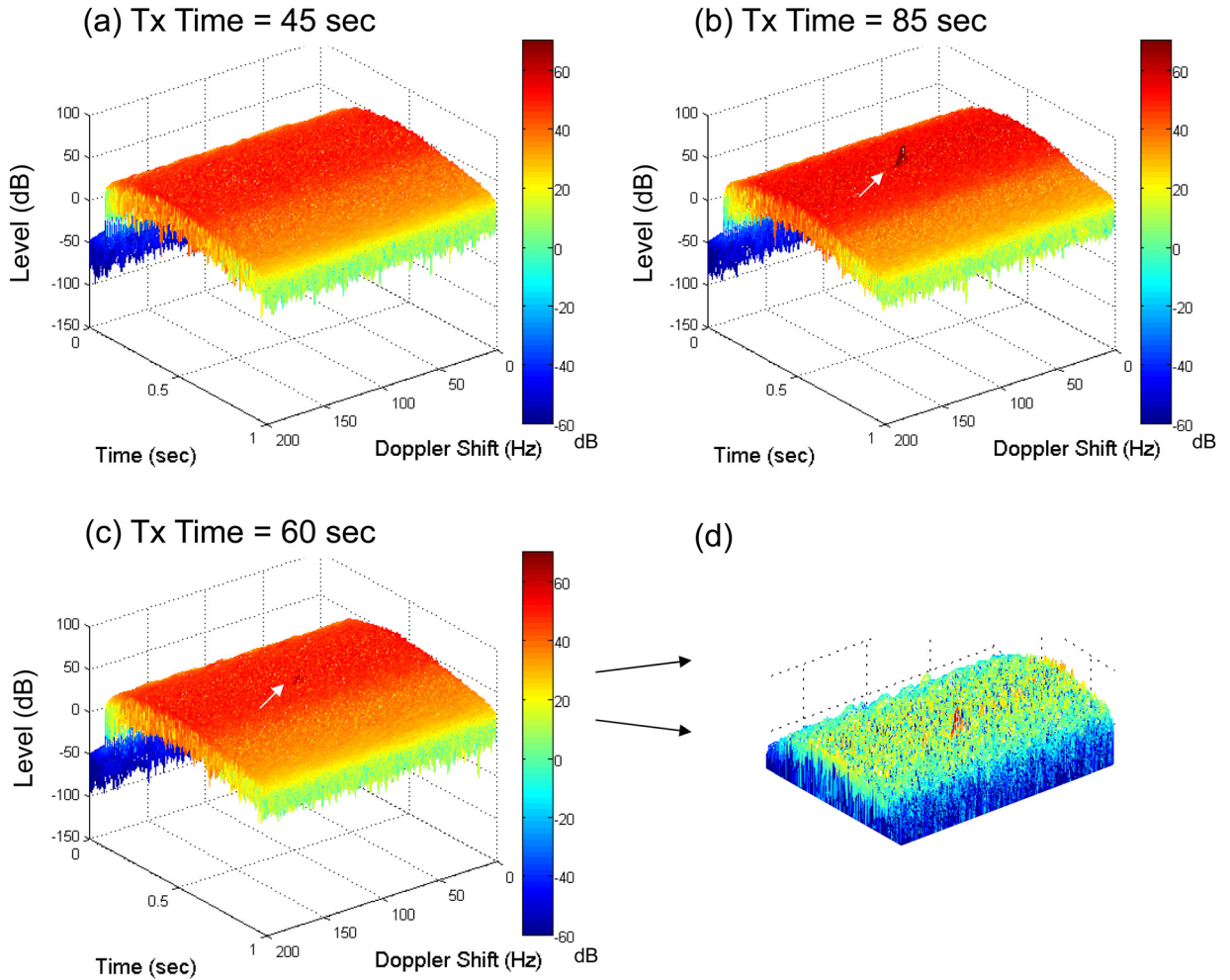


FIG. 14. (Color online) 3D view of the ambiguity surfaces for  $m$ -sequence signals transmitted at different times. (a) Signal not detected. (b) Signal detected. (c) Early detection of a weak signal. (d) Zoom in display of the signal in (c).

While the echo levels vary from ping to ping, in general the echo levels have the same order of magnitudes using different signal waveforms because they were transmitted with approximately the same energy.<sup>18</sup> For target detection at a given detection threshold, the probability of detection is determined by the signal excess; the higher the signal excess, the higher the probability of detection. Given a  $P_{fa} \sim 0.01$ , one determines a (detection) threshold of  $-10$  dB for the  $m$ -sequence data, and a threshold of  $-2$  dB for the LFM data as discussed in Sec. VI A. As a result, the signal excess is  $8$  dB larger using the  $m$ -sequence signal (with Doppler processing) than using the LFM signal. The difference in the signal excess can have significant consequences for target detection (the details depend on the probability of detection which is not measured in this experiment).

One observes in Fig. 5 that target detection and localization can be ambiguous in the presence of discrete high-level backscattered returns without first tracking the target. What makes detection and localization difficult is the peak reverberation level in the neighborhood of the target, which can be misidentified as a target. For comparison, we estimate the peak reverberation level in the neighborhood of the echo arrival time (within  $\pm 25$  ms of the target echo, excluding the

target echo). The result is shown in Figs. 13(a) and 13(b) using the data from Figs. 4 and 8, respectively. One observes that the SPRR is at times improved by  $>10$  dB using Doppler processing (comparing the  $m$ -sequence versus the LFM results). Note that the signal to reverberation ratio is, to a large extent, independent of the source level in a reverberation limited environment.

The improved SPRR is evident in the Dopplergram (Fig. 7) due to the low reverberation background. One can determine the SPRR following the second method mentioned in Sec. IV, based on the Dopplergram (Fig. 7). Using this method, the peak reverberation level can be estimated from the reverberation level over an area at, say, several Hertz away, from the target track. The result is approximately the same as that shown in Fig. 13(b).

One notes that the target echo level has a  $\sim 10$  dB drop in Fig. 13(b) after a round trip delay time of  $\sim 0.22$  s preventing target detection beyond this time. The reason for such a drop is not understood. If the decrease in target echo level is due to decreased processing gain (due to, e.g., decrease of coherence time with range), one expects the drop to be gradual with respect to range. It is suspected that the drop is amplifier related due to the higher duty cycle caused by the longer time duration of the  $m$ -sequence signal.

### C. Early warning

Detection based on first tracking the target (track before detect) may require many pings and extensive data processing. For defense against underwater swimmers, due to their limited speed, delayed detection may not be a problem since there is sufficient time to take action. Harbor protection is also concerned with the protection of valuable assets (ships) against underwater vehicles carrying high explosives, which can cause great damage. For a fast approaching object, delayed detection and high false alarm rates cannot be tolerated since time is critical, and a missed decision may carry grave consequences. One needs an early warning system which can detect the intruder with high confidence based on a single or a few snapshots of data. The Doppler-delay ambiguity surfaces, as shown in Fig. 14, for selected pings, may serve as an early warning tool. To do so, the ambiguity surfaces must cover a wide range of delay and Doppler based on possible target ranges and speeds. Looking at Fig. 14(a), the target echo was not detected at Tx Time of 45 s. Figure 14(a) reflects essentially the background level of the reverberation in the delay-Doppler space. The presence of a target is unambiguous at Tx Time = 85 s as shown in Fig. 14(b). The target is initially detected at Tx Time of 60 s [Fig. 14(c)], as indicated by a small peak (with  $>5$  dB SPRR) in the ambiguity surface. A detailed look of the target in Fig. 14(c) is given in Fig. 14(d). The above ambiguity surfaces were obtained by searching for the Doppler shift between 0 and 200 Hz, at a 2 Hz interval. The presence of a high peak (with SPRR  $>10$  dB) in the ambiguity surface with a Doppler shift greater than say 5 Hz, is a positive indication of a moving target since reverberation/clutter is concentrated at low Doppler frequencies. The results suggest that the wideband ambiguity surface can be used for early warning based on a small number of ping data.

As remarked earlier in Sec. III B, for the  $m$ -sequence signal, the main lobe of the wideband ambiguity surface has a very narrow width in the delay time ( $<1$  ms) and Doppler ( $\sim 3$  Hz). The target is not seen in the color display unless one zooms in to a time window on the order of 10 ms or less, due to limited number of pixels in a color display. The same is found in the real data (Fig. 6). For this reason, the three-dimensional (3D) display as shown in Fig. 14 is preferred for early warning or target detection. One can always display the target impulse response using the color display after the target is detected and localized. The measured impulse response can, in principle, be used to estimate the target depth. This topic is beyond the scope of this paper.

## VII. SUMMARY AND CONCLUSIONS

The Doppler properties of the target echo and reverberation are analyzed in this paper based on data collected in the Woods Hole Harbor. One finds that: (1) The matched filtered outputs using the LFM signal show many high level back-scattered returns (clutter) in the target look direction that are not target related. (2) Using the Doppler sensitive waveforms, the target and clutter show up with different Doppler. The clutter is found to have a negative Doppler shift of  $-10$  to  $0$  Hz with respect to the carrier frequency, or equivalently

a speed of  $\sim 0.15$  m/s moving away in the target look direction. A plausible cause for the low Doppler clutter is back-scattering returns from debris/fishes/shrimps carried by the tidal currents in the harbor. They are referred to as volume reverberation. (3) Target and clutter can be separated using Doppler processing. Target and clutter can be tracked using Dopplergram. (4) The high level volume reverberation returns have a non-Rayleigh (heavy-tailed) amplitude distribution. (5) The background reverberation after Doppler filtering has, in general, a low level Rayleigh-like amplitude distribution. (6) The Doppler filtered time series shows a much higher SPRR than that found in the LFM data. This is due to the fact that the clutter has largely been removed. (7) The wideband ambiguity surface using Doppler sensitive waveforms can be used to detect a moving target based on individual ping data due to the low (residue) reverberation level in the high Doppler space. The target speed can be used as a cue for early warning.

In this study we have used  $m$ -sequence signal due to its excellent (cyclic orthogonal) auto-correlation property which is responsible for the low sidelobe levels in the wideband ambiguity surface. Selected  $m$ -sequences also have good cross-correlation properties (at arbitrary delay), yielding minimal inter-sequence interference as demonstrated in code-division multiple-accessing underwater acoustic communications.<sup>21</sup> This suggests that multiple active sonar systems can be distributed around the harbor, pointing at different directions, transmitting different  $m$ -sequence signals that are orthogonal to each other. The advantages are that they can be operated simultaneously with minimal interference from other transmitted signals.

## ACKNOWLEDGMENT

The work by T.C.Y. and J.S. was supported by the US Office of Naval Research. The work by C.-F.H. and J.-Y.L. was supported by the National Science Council of Taiwan through Contract Nos. 98-2611-M-002-017-MY3 and 99-2221-E-110-093 and by the Ministry of Education of Taiwan.

<sup>1</sup>K. Shaw, R. Scott, and G. Holdanowicz, "Sonar sentinels on guard for submerged swimmers," *Jane's Navy International* (Sept. 2005).

<sup>2</sup>R. T. Kessel and R. D. Hollett, "Underwater intruder detection sonar for harbor protection: State of the art review and implications," in *Proceedings of the 2nd IEEE International Conference on Technologies for Homeland Security and Safety*, Istanbul, Turkey, October 2006. Reprint appeared in NURC-PR-2006-027. See Fig. 1.

<sup>3</sup>S. Coraluppi and C. Carthel, "Advances in active sonar tracking," in *Proceedings of the 14th European Signal Processing Conference*, Florence, Italy (September 2006).

<sup>4</sup>L. D. Stone, C. A. Barlow, and T. L. Corwin, *Bayesian Multiple Target Tracking* (Artech House, Boston MA, 1999), pp. 1–292.

<sup>5</sup>Y. Doisy, L. Deruaz, S. P. Beerens, and R. Been, "Target Doppler estimation using wideband frequency modulated signals," *IEEE Trans. Signal Process.* **48**, 1213–1224 (2000).

<sup>6</sup>Y. Doisy, L. Deruaz, S. van IJsselmuide, S. Beerens, and R. Been, "Reverberation suppression using wideband Doppler-sensitive pulses," *IEEE J. Ocean. Eng.* **33**, 419–433 (2008).

<sup>7</sup>G. Jourdain and J. P. Henrioux, "Use of large bandwidth-duration binary shift keying signals in target delay Doppler measurements," *J. Acoust. Soc. Am.* **90**, 299–309 (1991).

<sup>8</sup>J. P. Henrioux and G. Jourdain, "Use of large bandwidth-duration binary shift keying signals for bearing measurements in active sonar classification," *J. Acoust. Soc. Am.* **90**, 1737–1746 (1995).

- <sup>9</sup>T. C. Yang, "Acoustic Dopplergram for intruder defense," in *Proceedings of Oceans 2007*, Vancouver, BC (Oct. 2007).
- <sup>10</sup>A. W. Rihaczek, "Delay-Doppler ambiguity function for wideband signals," *IEEE Trans. Aerosp. Electron. Syst.* **3**, 705–711 (1967).
- <sup>11</sup>Z. Lin, "Wideband ambiguity function of broadband signals," *J. Acoust. Soc. Am.* **83**, 2108–2116 (1988).
- <sup>12</sup>J. P. Hermand and W. I. Roderick, "Delay-Doppler resolution performance of large time-bandwidth-product linear FM signals in a multipath ocean environment," *J. Acoust. Soc. Am.* **84**, 1709–1727 (1988).
- <sup>13</sup>See, for example, T. H. Eggen, A. B. Bagherer, and J. C. Preisig, "Communication over Doppler spread channels. Part I: Channel and receiver presentation," *J. Oceanic Eng.* **25**, 62–71 (2000), and T. C. Yang and W.-B. Yang, "Low probability of detection underwater acoustic communications using direct-sequence spread spectrum," *J. Acoust. Soc. Am.* **124**, 3632–3647 (2008).
- <sup>14</sup>W. J. Gill, "Effect of synchronization error in PR carrier communication," in *First Annual IEEE Comm. Conv. Conference Record*, Denver, June 7–9, pp. 187–191 (1965).
- <sup>15</sup>T. G. Birdsall, R. M. Heitmeyer, and K. Metzger, "Modulation by linear maximal shift register sequences: Amplitude biphase and complement phase modulation," Cooley Electronics Lab. Tech. Rep. 215 (1971), 35 p.
- <sup>16</sup>H. A. DeFerrari, H. Nguyen, and A. Rogers, "A low-power, high-resolution Doppler sonar for shallow water," in *Proceedings of New Concepts for Harbour Protection, Littoral Security and Shallow-Water Acoustic Communications*, Istanbul, Turkey, pp. 39–46 (2005).
- <sup>17</sup>T. C. Yang, J. Schindall, C.-F. Huang, and J.-Y. Liu, "Underwater-intruder detection in harbor environments using Dopplergram," in *Proceedings of the 10th European Conference on Underwater Acoustics (ECUA 2010)*, pp. 1357–1664 (July 2010).
- <sup>18</sup>The LFM and *m*-sequence signal amplitudes were adjusted during transmission to assure that they have the same energy. In actuality, the LFM has 0.9 dB higher energy than the *m*-sequence signal.
- <sup>19</sup>M. B. Porter and H. P. Bucker, "Gaussian beam tracing for computing ocean acoustic fields," *J. Acoust. Soc. Am.* **82**, 1349–1359 (1987).
- <sup>20</sup>Alternatively, one can use split-window normalization, i.e., normalized by the square root of the average energy of the adjacent windows. When many clutters are present in the data, split-window normalization tends to highlight the clutter more than the target.
- <sup>21</sup>T. C. Yang and W.-B. Yang, "Interference suppression for code-division multiple-access communications in an underwater acoustic channel," *J. Acoust. Soc. Am.* **126**, 220–228 (2009).